Colloidal Synthesis of Luminescent Rhabdophane $LaPO_4:Ln^{3+}\cdot xH_2O$ (Ln = Ce, Tb, Eu; $x \approx 0.7$) Nanocrystals

Valérie Buissette,† Mélanie Moreau,† Thierry Gacoin,† Jean-Pierre Boilot,*,†
Jean-Yves Chane-Ching,‡ and Thierry Le Mercier‡

Groupe de Chimie du Solide, Laboratoire de Physique de la Matière Condensée, CNRS UMR 7643, École Polytechnique, 91128 Palaiseau Cedex, and Centre de Recherches d'Aubervilliers, Rhodia, 52 rue de la Haie Coq, 93308 Aubervilliers, France

Received April 27, 2004

Lanthanide phosphate nanocrystals exhibiting the rhabdophane-type structure and mean particle sizes below 10 nm are synthesized by hydrolysis of an aqueous mixture of sodium tripolyphosphate ($Na_5P_3O_{10}$) and lanthanide salts. ^{31}P NMR studies show that polyphosphate groups act both as a source of orthophosphate and as complexing agents to, respectively, crystallize and stabilize $LnPO_4\cdot xH_2O$ ($x \approx 0.7$) nanoparticles. In the ternary system (Ln = La, Ce, and Tb), polyphosphate-capped particles form well-dispersed and highly luminescent aqueous colloids which are promising for applications in light-emitting devices.

Introduction

Recently, the study of nanometric luminescent materials has become of great interest.[1] First, the microstructural characteristics of the phosphors, such as the size or the surface properties of the grains, play an important role in the efficiency of luminescent devices. Second, new developments such as electroluminescent devices, integrated optics, or biological labels[2] imply the development of new phosphors whose properties can be managed at the nanometric scale.

Most studies have been focused on semiconductor nanocrystals such as CdSe quantum dots.[3] However, a significant amount of research has been recently devoted to doped insulators such as lanthanide-doped nanocrystals.[4] Concerning the synthesis of well-dispersed colloids, several research groups have reported on the doping of yttrium vanadate,[5,6] lanthanum fluoride,[7] lanthanum phosphate,[8] and yttrium oxide[9] nanoparticles with ions of the f elements.

The choice of the lanthanum phosphate was made because of the excellent luminescent properties of the bulk matrix when codoped with cerium and terbium ions.[10] This material is extensively used in fluorescent lamps as the green phosphor.[11] The green luminescence of the terbium ions is observed after a UV excitation of the cerium ions at the optimum wavelength of 272 nm. The excitation can further migrate from cerium to cerium until it reaches a terbium luminescent center. In the case of the $LaPO_4$ monazite bulk matrix, this mechanism is particularly efficient, and high emission yields, up to 93%, are obtained.[12] It has been recently shown that this green phosphor, and more generally lanthanide-doped $LaPO_4$ compounds exhibiting the monazite-type structure, can be obtained as colloids either in water or in high-boiling-point coordinating solvents.[8]

We present here a new aqueous colloidal synthesis of lanthanide phosphate nanoparticles $LnPO_4\cdot xH_2O$, where Ln = La, Ce, Tb, and Eu, based on the use of lanthanide salts and sodium polyphosphate precursors in water. The principle of this synthesis is the use of polyphosphate both as a source of orthophosphate ions (PO_4^{3-}) and as a stabilizing agent. Aging of a lanthanide−polyphosphate aqueous complex at 90 °C leads to the formation of colloidal nanoparticles of $LnPO_4\cdot xH_2O$ exhibiting the rhabdophane-type structure and mean particle sizes below 10 nm. Absorption and luminescence properties of $LnPO_4\cdot xH_2O$ lanthanide

* To whom correspondence should be addressed. E-mail: jean-pierre.boilot@polytechnique.fr.
† École Polytechnique.
‡ Rhodia.

(1) Jüstel, T.; Nikol, H.; Ronda, C. *Angew. Chem., Int. Ed.* **1998**, *37*, 3084.
(2) Chan, W. C.; Nie, S. M. *Science* **1998**, *281*, 2013.
(3) (a) Peng, X.; Schlamp, M. C.; Kadavanich, A.; Alivisatos, A. P. *J. Am. Chem. Soc.* **1997**, *119*, 7019. (b) Counio, G.; Gacoin, T.; Boilot, J.-P. *J. Phys. Chem. B* **1998**, *102*, 5257. (c) Murray, C. B.; Norris, D. J.; Bawendi, M. G. *J. Am. Chem. Soc* **1993**, *115*, 8706.
(4) (a) Tissue, B. M. *Chem. Mater.* **1998**, *10*, 2837. (b) Capobianco J. A.; Vetrone, F.; Boyer, J. C.; Speghini, A.; Bettinelli, M. *J. Phys. Chem. B* **2002**, *106*, 1181.
(5) (a) Huignard, A.; Gacoin, T.; Boilot, J.-P. *Chem. Mater.* **2000**, *12*, 1090−1094. (b) Huignard, A.; Buissette, V.; Laurent, G.; Gacoin, T.; Boilot, J.-P. *Chem. Mater.* **2002**, *14*, 2264−2269. (c) Huignard, A.; Buissette, V.; Franville, A.-C.; Gacoin, T.; Boilot, J.-P. *J. Phys. Chem. B* **2003**, *107*, 6754−6759. (d) Buissette, V.; Huignard, A.; Gacoin, T.; Boilot, J.-P, Aschehoug, P.; Viana, B. *Surf. Sci.* **2003**, *532*−*535*, 444−449.
(6) Riwotzki, K.; Haase, M. *J. Phys. Chem. B* **1998**, *102*, 10129.
(7) (a) Stouwdam, J. W.; Van Veggel, F. C. J. M. *Nano Lett.* **2002**, *2*, 7, 733−737. (b) Stouwdam, J. W.; Hebbink, G. A.; Huskens, J.; Van Veggel, F. C. J. M. *Chem. Mater.*, in press.
(8) (a) Riwotzki, K.; Meyssamy, H.; Schnablegger, H.; Kornowski, A.; Haase, M. *Angew. Chem., Int. Ed.* **2001**, *40*, 3, 573. (b) Meyssamy, H.; Riwotzki, K.; Kornowski, A.; Naused, S.; Haase, M. *Adv. Mater.* **1999**, *11*, 10, 840.
(9) Bazzi, R.; Flores-Gonzales, M. A.; Louis, C.; Lebbou, K.; Dujardin, C.; Brenier, A.; zhang, W.; Tillement, O.; Bernstein, E.; Perriat, P. *J. Lumin.* **2003**, *102*−*103*, 445−450.
(10) Blasse, G.; Grabmeier, B. C. *Luminescent Materials*; Springer-Verlag: New York, 1994.
(11) Maestro, P.; Huguenin, D. *J. Alloys Compd.* **1995**, *225*, 520.
(12) (a) Ropp, R. C. *J. Electrochem. Soc.: Solid State Sci.* **1968**, *115* (8), 841. (b) Bourcet, J.-C.; Kong, F. K. *J. Chem. Phys.* **1974**, *60* (1), 34. (c) Smets, B. M. J. *Mater. Chem. Phys.* **1987**, *16*, 283−299.

10.1021/cm049323a CCC: $27.50
Published on Web 08/27/2004

phosphate nanoparticles are studied in detail. Cerium and terbium ions are used as local probes to characterize both the growth of the lanthanide phosphate structure and the energy transfers inside the nanoparticles.[13]

Experimental Section

Synthesis of $LnPO_4 \cdot xH_2O$ Nanoparticles. The whole synthesis was carried out in water at 90 °C. A 0.1 mol·L^{-1} solution of $La(NO_3)_3$ (10 mL, 1 mmol) was mixed with a 0.1 mol·L^{-1} solution of sodium tripolyphosphate ($Na_5P_3O_{10}$, noted TPP) (10 mL, 1 mmol). The clear and colorless resulting mixture was subsequently aged at 90 °C for 3 h. The resulting lanthanum phosphate colloidal suspension was cooled and dialyzed for 1 day against deionized water to remove the excess of ions and phosphate species. This led to a transparent colloidal solution. To increase the stability of concentrated solutions, a 0.1 M solution of sodium hexametaphosphate [$(NaPO_3)_{12-13} \cdot Na_2O$] (2 mL, 0.2 mmol) was eventually added, and the colloid was further dialyzed for 3 days.

Lanthanide chloride was used instead of nitrate for UV−vis characterizations. Lanthanum salt was replaced by mixed (La, Ce, Tb or La, Eu) salts for the synthesis of luminescent nanoparticles. Powders of nanocrystals were obtained by evaporation of water under mild conditions (40 °C, 5 Torr).

Characterizations. Liquid-state ^{31}P NMR characterizations of colloids were achieved on a Bruker MSL 360 spectrometer operating at 145.786 MHz. H_3PO_4 (85%) was taken as a reference for the ^{31}P chemical shift. All NMR experiments were conducted with lanthanum compounds, to avoid the effects of paramagnetic lanthanide ions. The peak areas were measured using a Na_3PO_4 reference as a sealed tube placed in the sample. Acquisition parameters were optimized for the observations of either both liquid and colloidal species or only liquid species. The 90° pulse length was 25 μs. First, the dwell time (10 μs) and the dead times (25 μs) were reduced to the minimum acceptable to detect phosphorus atoms in small solid species with shorter decay times. Second, they were set to 34 and 40 μs, respectively, to selectively observe liquid species. The recycle decay was set to 10 s, and a total of 64 spectra were recorded.

^{31}P MAS NMR characterizations of powders were achieved on the same spectrometer with a spinning frequency of 15 kHz. The 90° pulse length was 5.5 μs, the dwell time was 30 μs, and the recycle decay was 150 s. A total of four scans were recorded.

Phosphorus and lanthanide atomic contents in nanoparticles were deduced from chemical analysis performed by inductively coupled plasma emission spectrometry (ICP-ES) after dissolution of nanoparticles in HNO_3 (70%). Since the presence of Ce^{4+} ions quenches the luminescence of Ce^{3+} and thus alters the luminescence of the LaCeTb-codoped systems,[14] it was checked by absorption spectrometry that the Ce^{4+} content was lower than 1% in these nanoparticles.

Dynamic light scattering experiments were carried out with PCS (photon correlation spectroscopy) light scattering equipment supplied by Malvern. Absorption spectra were recorded on a Schimidazu 160 A spectrophotometer. X-ray diffraction (XRD) studies were performed on the powders of nanocrystals using a Philips X-Pert diffractometer with Cu Kα radiation (λ = 154 pm). A Netzsch thermoanalyzer, STA 409, was used for simultaneous thermal analysis combining thermogravimetry (TG) and differential thermal analysis (DTA) with a heating rate of 10 °C·min^{-1} in air. Transmission electron spectroscopy (TEM) was performed on a Philips CM 30 microscope operating at 300 kV. Samples were prepared by depositing a droplet of colloidal solution on a carbon film.

Luminescence spectra and lifetime measurements were recorded on a Hitachi F-4500 spectrofluorometer. The quantum yields were determined by comparing the integrated emission of the scatter-free colloidal solutions with the emission of a Rhodamine 6G solution in ethanol having the same optical density (OD < 0.3) and excited at the same wavelength. As previously suggested,[15] the emission of a quinine bisulfate solution in H_2SO_4 (1 M) can also be a reference to determine the luminescence quantum yield. The use of these two reference solutions has led to similar results within 5%.

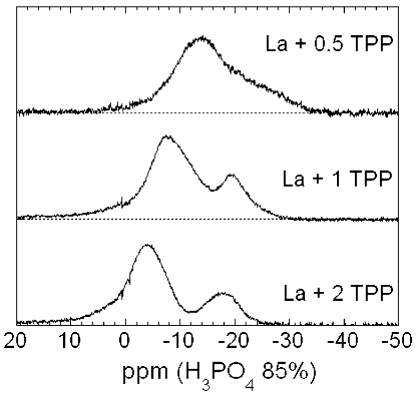

Figure 1. ^{31}P MAS NMR spectra of the TPP/La entities as a function of the TPP/La ratio.

Results and Discussion

Ln−TPP Precursor. In the starting mixture (TPP/La = 1), dynamic light scattering measurements indicate the presence of scattering species with a hydrodynamic diameter of 5 nm. The X-ray diagram (not shown) recorded on a powder after drying in mild conditions (40 °C under vacuum) shows that the compound is amorphous, suggesting the presence of colloidal polymeric species in the initial mixture. The ^{31}P liquid NMR spectrum of the mixture was recorded in experimental conditions where all the phosphorus atoms are detected. The spectrum (not shown) presents two peaks around −5 and −18 ppm corresponding to the two equivalent lateral and central phosphorus atoms of free TPP groups in solution. The integration of these peaks shows that they correspond to about 30% of the phosphorus atoms. Other TPP groups (about 70%) are included in polymeric species (solid phase) and appear as two broad bands in the NMR spectra.

^{31}P MAS NMR experiments were also performed on dried samples with different TPP/La ratios (Figure 1). The spectra present large bands characteristic of the broad distribution of environments around the phosphorus atoms in the solid phase. This is in agreement with the amorphous structure observed in the X-ray pattern. The local environments around the phosphorus atoms are clearly dependent on the TPP/La ratio as revealed by the progressive evolution of the ^{31}P chemical shift. This provides a calibration in La/TPP ratios, which will be later used to characterize the surface complexation of the grown lanthanide phosphate nanoparticles.

Growth of Lanthanide Phosphate Nanoparticles from the Hydrolysis of TPP/Ln Mixtures. The principle of the synthesis of the nanoparticles in water consists of using a polyphosphate salt both as a source of orthophosphate[16] and as a complexing agent. Different polyphosphate groups $[P_nO_{3n+1}]^{(n+2)-}$ (n = 3, 12, and 25) were tested, leading to the same products with only

(13) Dorenbos, P. *Phys. Rev. B* **2001**, *64*, 125117.

(14) (a) Van Schaik, W.; Lizzo, S.; Smit, W.; Blasse, G. *J. Electrochem. Soc.* **1993**, *140*, 1, 216. (b) Lin, J.; Yao, G.; Dong, Y.; Park, B.; Su, M. *J. Alloys Compd.* **1995**, *225*, 124.

(15) Melhuish, W. H. *J. Phys. Chem.* **1960**, *64* (6), 762.

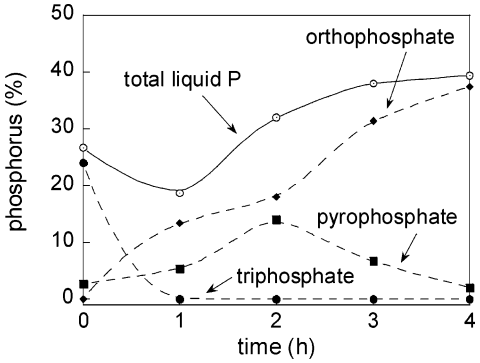

Figure 2. Time evolution of the proportion of the different phosphorus liquid species relative to the initial phosphorus concentation, deduced from liquid ^{31}P NMR data, after hydrolysis of the TPP/La = 1 mixture.

different kinetics. The tripolyphosphate chain ($n = 3$) was found to be a good compromise to ensure both the rapid formation of orthophosphate ions by hydrolysis and the stability of nanoparticles by complexation of the lanthanides.

In preliminary experiments, the aging at 90 °C of the TPP/Ln = 1 mixture was followed by recording liquid-state ^{31}P NMR spectra. In this case, $LaCl_3$ was used as a lanthanide salt, and the total concentration of P atoms was 0.15 M. The spectra were recorded in pure "liquid" experimental conditions (large delay times) to specifically and quantitatively detect the free species in the liquid phase.

Figure 2 shows the time evolution of the P liquid fraction for all (poly)phosphate groups. As previously noted before reaction, only 30% of the P atoms of the initial mixture are inside the liquid phase as free TPP species. The heating process activates the hydrolysis of the tripolyphosphate groups, which progressively turn into pyrophosphate ($P_2O_7^{4-}$) and orthophosphate (PO_4^{3-}) ions. After 1 h of aging, all the free TPP species are hydrolyzed, and the liquid fraction decreases to 20%, which suggests a progressive precipitation of lanthanum phosphate. In the same range, the orthophosphate concentration continuously increases in the liquid phase, suggesting a competition between the precipitation of lanthanum phosphate particles and the complexing action of the tripolyphosphate at their surface. By increasing the aging time, the orthophosphate ion concentration still increases in the liquid phase due to the hydrolysis of TPP groups belonging to the solid phase. After 4 h, about 40% of the phosphorus atoms are in orthophosphate groups in the liquid phase. The solution becomes more and more turbid due to a progressive aggregation of lanthanide phosphate particles.

The kinetics of the growth of lanthanide phosphates were studied by optical measurements on the colloidal species in solution. In the following experiments, lanthanide salts $(La_{40\%}Ce_{45\%}Tb_{15\%})Cl_3$ are mixed with 1 molar equivalent of sodium tripolyphosphate (TPP/Ln = 1) and further aged at 90 °C. Samples are then taken from the suspension at different times, cooled to stop the reaction, and then characterized by absorption and luminescence spectroscopies. The time evolution of the cerium absorption spectra and of the terbium-integrated luminescence (from 450 to 700 nm) are shown in Figure 3.

Concerning the starting mixture, the absorption bands observed at 248 and 302 nm are attributed to cerium−tripolyphosphate free complexes. The band at 272 nm which grows during the synthesis can be attributed to the cerium in the lanthanum phosphate phase. Assuming this, the intensity of the absorption band at 272 nm is directly related to the amount of crystalline lanthanide phosphate phase which is formed, whereas the intensity at 302 nm is related to the disappearance of the lanthanide−tripolyphosphate complexes. For the two bands, the time evolution of the intensity presents a plateau after 2 h of aging. At longer aging times, the residual contribution at 302 nm is due to cerium ions located either in a polyphosphate shell at the surface of the lanthanide phosphate crystals or in free TPP species. A calibration of the absorption coefficient of the cerium ions in the nanoparticles has been performed by coupling absorption and chemical analysis on well-purified 3 h grown lanthanide phosphate crystallites. The measured extinction coefficient is about 710 $L \cdot mol^{-1} \cdot cm^{-1}$ at 272 nm. This value is useful to measure the concentration of the lanthanide phosphate for further chemical treatments.

Growth kinetics of the lanthanide phosphate can also be monitored by the time evolution of the terbium luminescence under 272 nm excitation. This evolution is plotted in Figure 3b as a function of the aging time, and compared to the absorption at 272 nm. The plateau is reached after 1.5 h at 90 °C, and the luminescence of the terbium slightly increases for longer treatments. All these results tend to prove that a great part of the lanthanide phosphate phase is formed after 1.5 h in our experimental conditions.

These optical results can be correlated to the X-ray data obtained on powders. After different aging times,

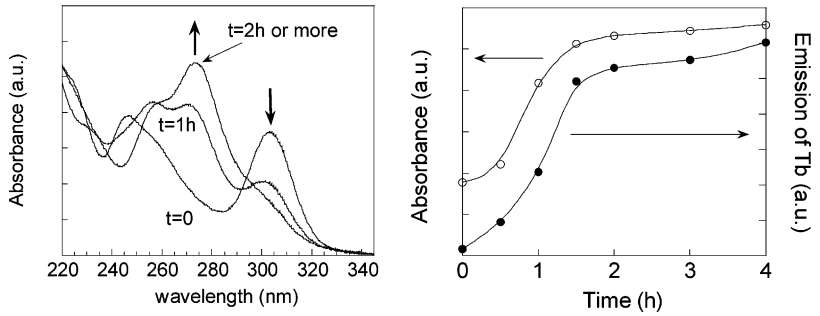

Figure 3. Growth of lanthanide phosphate particles by aging at 90 °C of polymeric precursor colloids (TPP/$(La_{40\%}Ce_{45\%}Tb_{15\%})Cl_3$ = 1). (a, left) Absorption spectra at $t = 0$, 1, and 2 h. (b, right) Time evolution of the Ce^{3+} absorption band at 272 nm and of the emission of Tb^{3+} under 272 nm excitation.

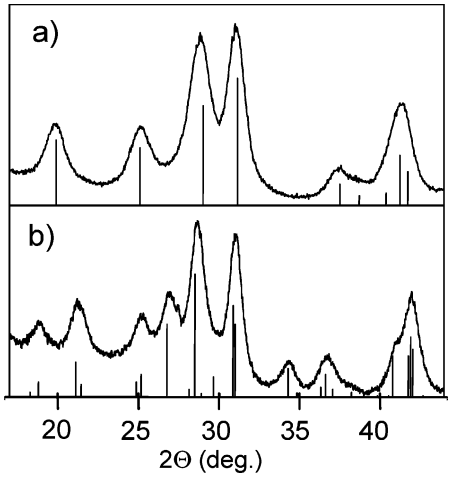

Figure 4. X-ray diagrams of lanthanum phosphate nanoparticles. (a) Crude nanoparticles with the $LaPO_4 \cdot xH_2O$ trigonal rhabdophane structure (PDF 46-1439). (b) Nanoparticles heated at 500 °C with the $LaPO_4$ monoclinic monazite structure (PDF 32-0493).

the solutions were further purified by dialysis and dried in mild conditions. For a time inferior to 1 h, no crystalline phase is observed on the X-ray pattern. For aging times higher than 1.5 h, diffraction peaks appear corresponding to the rhabdophane-type structure of lanthanum phosphate (see the structural characterization below). The diffraction coherence length, as deduced from the Williamson−Hall analysis, continuously increases from 3 nm for 1.5 h of aging at 90 °C to 10 nm for a 16 h aging. Since both absorption and luminescence results indicate that almost all the phosphate phase is formed after a reaction time of 1.5 h, a further increase of the coherence length of the particles can only result from an improvement of their crystallinity or a growth through an Ostwald ripening process.

Structure of 5 nm Nanoparticles. Figure 4 displays the powder diffraction diagram of lanthanum phosphate nanoparticles obtained after 3 h of aging at 90 °C. Despite the broadening caused by the small size of the particles (the coherence length was 5 nm), the pattern recorded at room temperature (Figure 4a) is in good agreement with the rhabdophane structure $LaPO_4 \cdot xH_2O$ (trigonal space group $P3_121$).[17] This low-temperature lanthanum phosphate phase is the same as the one obtained by simple mixing of La^{3+} and PO_4^{3-} salts in water at ambient temperature.[18] The hydration of the $LaPO_4$ crystal is due to zeolitic water present in the channel-type structure.

Figure 5 presents TG and DTA curves performed on the nanoparticle powder. The weight loss occurs in two steps. The first one below 200 °C corresponds to the release of water molecules adsorbed on the powder surface and is associated with an endothermic peak whose maximum is at 132 °C. The second, in the 200−450 °C range, corresponds to the progressive dehydration of the rhabdophane phase and is accompanied by

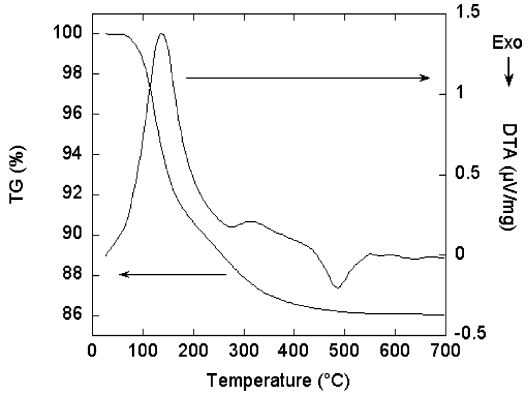

Figure 5. TG and DTA for hydrated lanthanum phosphate nanoparticles with the trigonal rhabdophane-type structure.

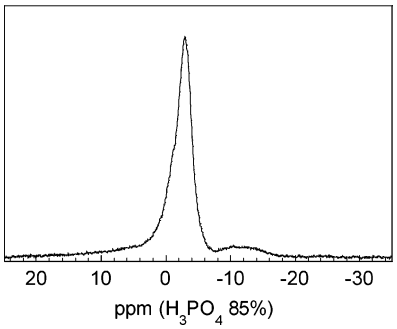

Figure 6. ^{31}P NMR MAS performed on a powder of lanthanum phosphate nanoparticles.

an endothermic broad band (maximum at 320 °C). The hydration ratio of the rhabdophane structure ($x \approx 0.7$) for crude nanoparticles is deduced from the weight loss measured during this second step.

At 480 °C, an exothermic peak is observed which is assigned to the structural transition from the rhabdophane to the monazite-type structure of $LaPO_4$. This is confirmed by the X-ray diagram performed on nanoparticles heated at 500 °C for 8 h in air (Figure 4b), which corresponds to the monazite structure with an average coherence length of 16 nm. This structural transition is also observed for bulk materials under various experimental conditions.[19]

The rhabdophane phase is also observed in X-ray patterns for $(La,Ce,Tb)PO_4$ nanoparticles. The hexagonal cell parameters are deduced from a structural refinement of the cell parameters for different compositions of the lanthanide phosphate crystallites: $a = 713.1$ pm and $c = 649.5$ pm for $LaPO_4 \cdot xH_2O$, $a = 706.3$ pm and $c = 644.5$ pm for $CePO_4 \cdot xH_2O$, and $a = 688.0$ pm and $c = 631.1$ pm for $TbPO_4 \cdot xH_2O$. For all the intermediary compositions, Vegard's law (not shown) is verified, i.e., the linear evolution of the unit cell volume, showing the existence of a complete solid solution in the $(La,Ce,Tb)PO_4 \cdot xH_2O$ nanoparticles.

The nanoparticle powder was also studied by ^{31}P MAS NMR (Figure 6). The spectrum presents the peak characteristic of the hydrated rhabdophane phase at around −3.2 ppm (instead of −4.5 ppm for the dehydrated monazite phase)[18b] and broad bands correspond-

(16) (a) Corbridge, D. E. C. *Phosphorus 2000: Chemistry, Biochemistry and Technology*; Elsevier: New York, 2000. (b) Crowther, J. P.; Westman, A. E. R. *Can. J. Chem.* **1954**, *32*, 42−48.

(17) Mooney, R. C. L. *Acta Crystallogr.* **1950**, *3*, 337.

(18) (a) Lucas, S.; Champion, E.; Bernache-Assollant, D.; Leroy, G. *J. Solid State Chem.* **2004**, *177*, 1312. (b) Glorieux, B.; Matecki, M.; Fayon, F.; Coutures, J. P.; Palau, S.; Douy, A.; Peraudeau. *J. Nucl. Mater.* **2004**, *326*, 156.

(19) (a) Hikichi, Y.; Hukuo, K.; Shiokawa, J. *Bull. Chem. Soc. Jpn.* **1978**, *51*, 12, 3645. (b) Jonasson, R. G.; Vance, E. R. *Thermochim. Acta* **1986**, *108*, 65. (c) Fujishiro, Y.; Ito, H.; Sato, T.; Okuwaki, A. *J. Alloys Compd.* **1997**, *252*, 103.

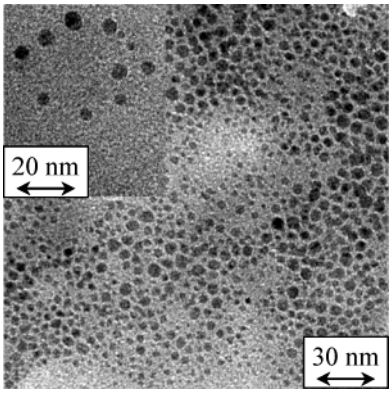

Figure 7. TEM of the TPP-capped lanthanum phosphate nanoparticles. Statistics from 420 nanoparticles leads to an average size of 3.9 nm (standard deviation 1.3 nm).

ing to polymeric species. After measurement of the T_1 relaxation times, the acquisition conditions were chosen to have a quantitative view of phosphorus species, which implies very long decay times ($D_0 = 150$ s). By a simple fit and using the previous calibration of Figure 1, it can be shown that the remaining polymeric species are located around −0.5 ppm (lanthanum pyrophosphate (La−PP) with a PP/La ratio between 0 and 1) and −13 and −24 ppm (lanthanum tripolyphosphate (La−TPP) with a TPP/La ratio between 0.5 and 1). The relative amounts of phosphorus atoms in the different phases are thus the following: 85% of the P atoms in crystalline $LaPO_4 \cdot 0.7H_2O$ and 15% of the P atoms in the surface polymeric shell (9% of the P atoms in La−TPP and 6% in La−PP). Chemical analysis on these particles attests a P/Ln ratio of 1.3, which confirms the excess of phosphorus atoms at the surface of the particles as shown by NMR data.

Unlike liquid species, where all the tripolyphosphate groups are hydrolyzed, it seems that unhydrolyzed tripolyphosphate species are present at the surface of the nanoparticles. This can explain the effective control of the size of the nanoparticles during the growing process, and the good redispersion of the colloid after purification. A simple calculation combining chemical analysis, the size of the particles, and NMR data leads to the evaluation of the lanthanide ions present in the shell of the particles. They represent 5% of the total lanthanide ions.

To provide a better stabilization of the colloids at long times or to concentrate them, hexametaphosphate (0.2 molar equivalent with respect to the lanthanide) is added to the colloid at ambient temperature, and the excess is removed by dialysis against distilled water. After purification, a clear colloid (10 g/L) is obtained, with a mean hydrodynamic diameter of about 13 nm. Colloids can be further concentrated up to 50 g/L under mild conditions. A transmission electron micrograph displaying the size distribution of the colloid is given in Figure 7. The image shows well-dispersed lanthanum phosphate nanoparticles with an average size of 3.9 nm and a standard deviation of 1.3 nm.

Optical Properties of Nanoparticles. Figure 8 shows the typical absorption and excitation spectra of $LaPO_4$:Ce$\cdot x H_2O$ colloids. The broad bands, peaking at 254 and 272 nm, are ascribed to the 4f−4f5d absorption bands of the cerium in the rhabdophane matrix.[12] These

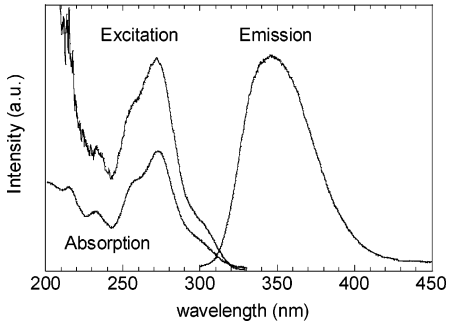

Figure 8. Excitation (em = 350 nm), absorption, and emission (ex = 272 nm) spectra for $LaPO_4$:$Ce_{33\%}\cdot x H_2O$ rhabdophane colloids in water.

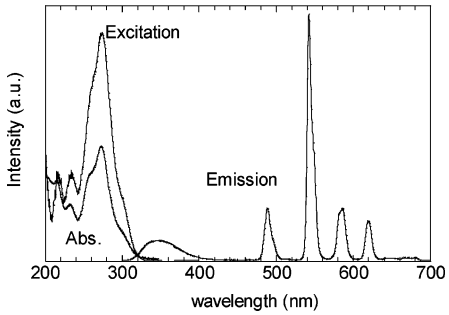

Figure 9. Excitation (em = 543 nm), absorption, and emission (ex = 272 nm) spectra for $LaPO_4$:$Ce_{45\%}Tb_{15\%}\cdot x H_2O$ colloids in water.

positions are only slightly shifted compared to those (258 and 274 nm) which have been previously observed in the case of lanthanide phosphate nanoparticles with a monazite-type stucture.[8]

The luminescence spectrum (Figure 8) presents a large emission band, centered at 345 nm. This band is red shifted compared with the luminescence signals observed for the monazite bulk material (315 nm) and for monazite nanoparticles (330 nm).[8] This emphasizes the fact that the d electrons of cerium couple differently to the lattice phonons in the rhabdophane structure, leading to a higher Stokes shift. Consequently, a violet luminescence of the colloid is observed with the naked eye. The luminescence quantum yield of the rhabdophane $LaPO_4$:$Ce_{33\%}\cdot x H_2O$ colloid in water is 70%.

Concerning $(La_{40\%}Ce_{45\%}Tb_{15\%})PO_4\cdot x H_2O$ nanoparticles (Figure 9), absorption and excitation spectra of the green luminescence (543 nm) are characteristic of the absorption of the 4f−4f5d bands of the cerium. The luminescence spectrum displays the typical line spectrum of the terbium $^5D_4 - ^7F_J$ transitions between 450 and 700 nm.[12] A significant contribution (about 30% of the total) is observed at 350 nm, due to cerium ions whose luminescence is not totally quenched, as was observed in monazite bulk and nanoparticles. The luminescence quantum yield is 31% for the green luminescence of the terbium and 43% if the cerium contribution is added. This is a high value for nanoparticles in water, which is intermediate between the 24% previously observed for the monazite-type nanoparticle in protic solvents and the 93% for the bulk monazite material.[8a]

As previously shown for YVO_4:Eu nanoparticles, lanthanide ions are well-known to be quenched by hydroxyl groups.[5] This is the case for terbium ions, where the $^5D_4$ emitting level is about 5 times the OH

vibration. After transfer of nanoparticles into deuterated water, the Tb quantum yield reaches 61%, and a total luminescence yield of 73% is obtained when cerium emission is included (instead of 42% for Tb emission and 61% including Ce emission for monazite nanoparticles in aprotic solvents).[8a] Note that cerium ions are less sensitive to OH quenching because of the higher energy levels. At the same time, the measured lifetime of the terbium (excitation at 272 nm, emission at 543 nm), which was 2.7 ms in water, reaches 5.4 ms in deuterated water. Both the rise of the quantum yield and that of the lifetime are consistent with a decrease of the nonradiative quenching of the terbium ions through the OH groups. In fact, it can be noted that the quantum yield obtained for $(La_{40\%}Ce_{45\%}Tb_{15\%})PO_4 \cdot xH_2O$ colloids in water is higher than that reported for monazite particles in protic solvents. This shows that the structural water molecules present in the channels of the rhabdophane structure do not significantly alter the luminescence properties and that most quenching by OH groups occurs at the surface of particles.

All these experiments were performed on $La_{40\%}Ce_{45\%}Tb_{15\%}$ nanoparticles whose composition is derived from studies of the bulk monazite material. It is known that, in nanoparticles, size and surface effects can alter energy-transfer processes so that the optimum cerium and terbium concentrations should be reinvestigated in the nanoparticles.[5c] As for the bulk, the best luminescence quantum yield of the terbium is obtained by dilution of the two luminescent ions in the $LaPO_4$ matrix, and the optimum concentrations in cerium and terbium ions are 45% and 15%, respectively. However, in this composition, the cerium emission in the UV−vis region represents about 30% of the total luminescence of nanoparticles. This indicates a lower efficiency of the cerium to terbium transfer in comparison with the bulk in which the cerium contribution to the luminescence is weak (7%).[14] To minimize the emission of the cerium in nanoparticles, it is necessary to increase the amount of terbium ions. Resulting from systematic variations by steps of 15%, optimum ionic concentrations leading to the highest Tb emission and to the lowest Ce emission are found to be 45% in cerium and 55% in terbium, i.e., without dilution in the $LaPO_4$ matrix. In this case, the emission of cerium represents 0.3% of the total emission, and the luminescence quantum yield is 22% in water and 62% in D_2O.

Finally, concerning the brightness of these colloids under excitation, it is necessary to take into account not only the emission yield but also the absorption coefficient to maximize the number of photons emitted by a nanoparticle. In the case of these green emitting colloids, the absorbing species are cerium ions, and the more the particles are doped, the more they absorb. The optimum composition is then deduced by considering the amount of cerium content multiplied by the emission yield of the terbium. In this case, the optimum concentrations are 85% cerium ions and 15% terbium ions. The global emission yield is 30% in water and 60% in D_2O; the fraction of cerium emission in water is 23%. This colloid is thus 1.4 brighter than for the usual $(La_{40\%}Ce_{45\%}Tb_{15\%})$ composition.

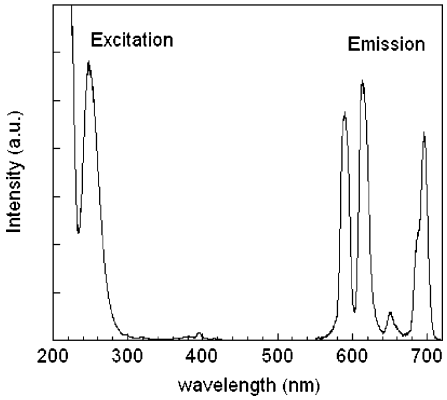

Figure 10. Excitation (em = 614 nm), absorption, and emission (ex = 260 nm) spectra for $LaPO_4:Eu_{10\%} \cdot xH_2O$ colloids in water.

Preliminary luminescence experiments have also been performed on $LaPO_4:Eu_{10\%} \cdot xH_2O$ rhabdophane red luminescent colloids (Figure 10). As previously observed for both Eu^{3+}-doped $LaPO_4$ bulk and nanocrystals, the absorption band below 300 nm is due to an oxygen to europium charge-transfer transition, and the main lines of the emission spectrum are due to transitions from the $^5D_0$ level of Eu^{3+}.[20]

The brightness of these colloids under UV excitation is significantly lower than that of the cerium−terbium-doped colloids, due to the low absorption cross-section of the charge-transfer band at 260 nm. Further experiments are required to determine more precisely the spectroscopic properties of these particles.

Conclusion

We have developed a new aqueous colloidal synthesis of lanthanide phosphate nanoparticles $LnPO_4 \cdot xH_2O$ ($x \approx 0.7$), where Ln = La, Ce, Tb, and Eu, based on the use of a mixture of lanthanide salts and TPP precursors in water. Hydrolysis of TPP groups and subsequent growth of lanthanide phosphate particles are observed after aging at 90 °C of the TPP/Ln = 1 transparent mixture. This leads to well-dispersed TPP-capped colloids of $LnPO_4 \cdot xH_2O$ ($x \approx 0.7$) exhibiting the rhabdophane type structure and average sizes below 10 nm.

The complete solid solution in the $(La,Ce,Tb)PO_4 \cdot xH_2O$ ternary system leads to highly luminescent well-dispersed colloids which exhibit bright violet (La, Ce) and green (La, Ce, Tb) luminescence under UV excitation. Preliminary experiments have also been performed on other lanthanide dopings such as Eu^{3+} doping, which has led to red luminescent colloids.

Luminescence properties of rhabdophane aqueous colloids appear as similar to those of monazite colloids in protic solvents, showing that the structural water molecules of the rhabdophane structure do not significantly alter the luminescence properties. The partial quenching of the luminescence observed in aqueous colloids is essentially related to OH groups located at the surface of particles.

Concerning green emitting colloids, and as previously demonstrated in the YVO_4:Eu system, luminescence

(20) Riwotzki, K.; Meyssamy, H.; Schnablegger, H.; Kornowski, A.; Haase, M. *J. Phys. Chem. B* **2000**, *104*, 2824.

experiments clearly reveal that the cerium to terbium energy-transfer efficiency is lower than that observed in the bulk. Further experiments are in progress to completely understand this result, which is probably associated with intrinsic characteristics of nanoparticles such as structural distortions or surface effects.

Acknowledgment. We are grateful to Guillaume Laurent for help during the NMR experiments. Chemical analysis experiments were performed at the Service Central d'Analyze du CNRS, Vernaison, France.

CM049323A